Charge, orbital and spin ordering phenomena in the mixed valence manganite $(NaMn^{3+}_3)(Mn^{3+}_2Mn^{4+}_2)O_{12}$

A. PRODI*[1], E. GILIOLI[1], A. GAUZZI[1], F. LICCI[1], M. MAREZIO[1], F. BOLZONI[1], Q. HUANG[2], A. SANTORO[2] AND J.W. LYNN[2]

[1]Istituto dei Materiali per Elettronica e Magnetismo-CNR, Area delle Scienze, 43010 Parma, Italy
[2]NIST Center for Neutron Research, National Institute of Standards and Technology, Gaithersburg, Maryland 20899, USA
*e-mail: prodi@imem.cnr.it

Published online: 14 December 2003; doi:10.1038/nmat1038

Mixed-valence manganites with the ABO_3 perovskite structure display a variety of magnetic and structural transitions, dramatic changes of electrical conductivity and magnetoresistance effects. The physical properties vary with the relative concentration of Mn^{3+} and Mn^{4+} in the octahedral corner-sharing network, and the proportion of these two cations is usually changed by doping the trivalent large A cation (for example, La^{3+}) with divalent cations. As the dopant and the original cation have, in general, different sizes, and as they are distributed randomly in the structure, such systems are characterized by local distortions that make it difficult to obtain direct information about their crystallographic and physical properties. On the other hand, the double oxides of formula $AA'_3Mn_4O_{12}$ contain a perovskite-like network of oxygen octahedra centred on the Mn cations, coupled with an ordered arrangement of the A and A′ cations, whose valences control the proportion of Mn^{3+} and Mn^{4+} in the structure. The compound investigated in this work, $(NaMn^{3+}_3)(Mn^{3+}_2Mn^{4+}_2)O_{12}$, contains an equal number of Mn^{3+} and Mn^{4+} in the octahedral sites. We show that the absence of disorder enables the unambiguous determination of symmetry, the direct observation of full, or nearly full, charge ordering of Mn^{3+} and Mn^{4+} in distinct crystallographic sites, and a nearly perfect orbital ordering of the Mn^{3+} octahedra.

In the early 1970s, while searching for a high-pressure phase of Mn_2O_3 and MnOOH, a new compound was obtained[1], which proved to be $(NaMn_3)Mn_4O_{12}$. The chemical formula and the structure showed that it was isostructural with $(CaCu_3)Ti_4O_{12}$, first reported[2] in 1964. During the 1970s, several other oxides with the general formula $AA'_3B_4O_{12}$ were synthesized and characterized[3]. These ternary oxides possess a cubic structure whose unit cell consists of four perovskite blocks. The B sublattice together with that of oxygen makes up the three-dimensional corner-sharing octahedral network of the perovskite structure, and the A and A′ cations occupy 12-coordinated crystallographically independent sites in an ordered fashion. In 1975 it was reported that $(NaMn_3)Mn_4O_{12}$ undergoes a crystallographic transition at 180 K where the crystal symmetry changes from cubic to monoclinic, inducing a splitting of the octahedral Mn lattice into two sublattices. It was argued that this was due to the Mn charge ordering[4], but no analysis of the structural and magnetic properties of the compound was carried out.

Samples of $(NaMn_3)Mn_4O_{12}$ were synthesized under pressure in a multi-anvil apparatus. The samples were studied by powder X-ray diffraction using a commercial diffractometer equipped with Cu K_α radiation. The X-ray diffractograms indicate that the samples are better than 96% pure, with Mn_2O_3 as the main impurity. The least-squares refinements of the unit cell parameters yielded values close to those reported[1], and consistent with the *Im*3 space group. All structural refinements of the nuclear and magnetic structures were carried out using neutron powder-diffraction data. The neutron profiles and refined structural details are included in the Supplementary Information (see Figs S1, S2 and Tables S1–S3, respectively). The room-temperature structure of $(NaMn_3)Mn_4O_{12}$ (Fig.1) was refined in space group *Im*3 ($a = 7.3043(3)$ Å with Na located at (0,0,0), Mn(1) at (0, 1/2, 1/2), Mn(2) at (1/4, 1/4, 1/4) and O at (0.3131(4), 0.1824(4),0)), with excellent agreement between observed and calculated intensities (powder residual, $R_p = 4.34\%$; weighted R_p, $wR_p = 5.22\%$; $\chi^2 = 0.82$). As shown in Fig. 2, the value of the lattice parameter remains practically constant with decreasing temperature, until peaks of a new phase appear below 176 K. These new peaks coexist with those of the high-temperature cubic structure over the limited range between 176 K and 168 K, whereas below 168 K the transition is complete and only the new structure is present. This behaviour is in sharp contrast to that observed in $La_{1/2}Ca_{1/2}MnO_3$, where the low-temperature phase ($T < 230$ K)

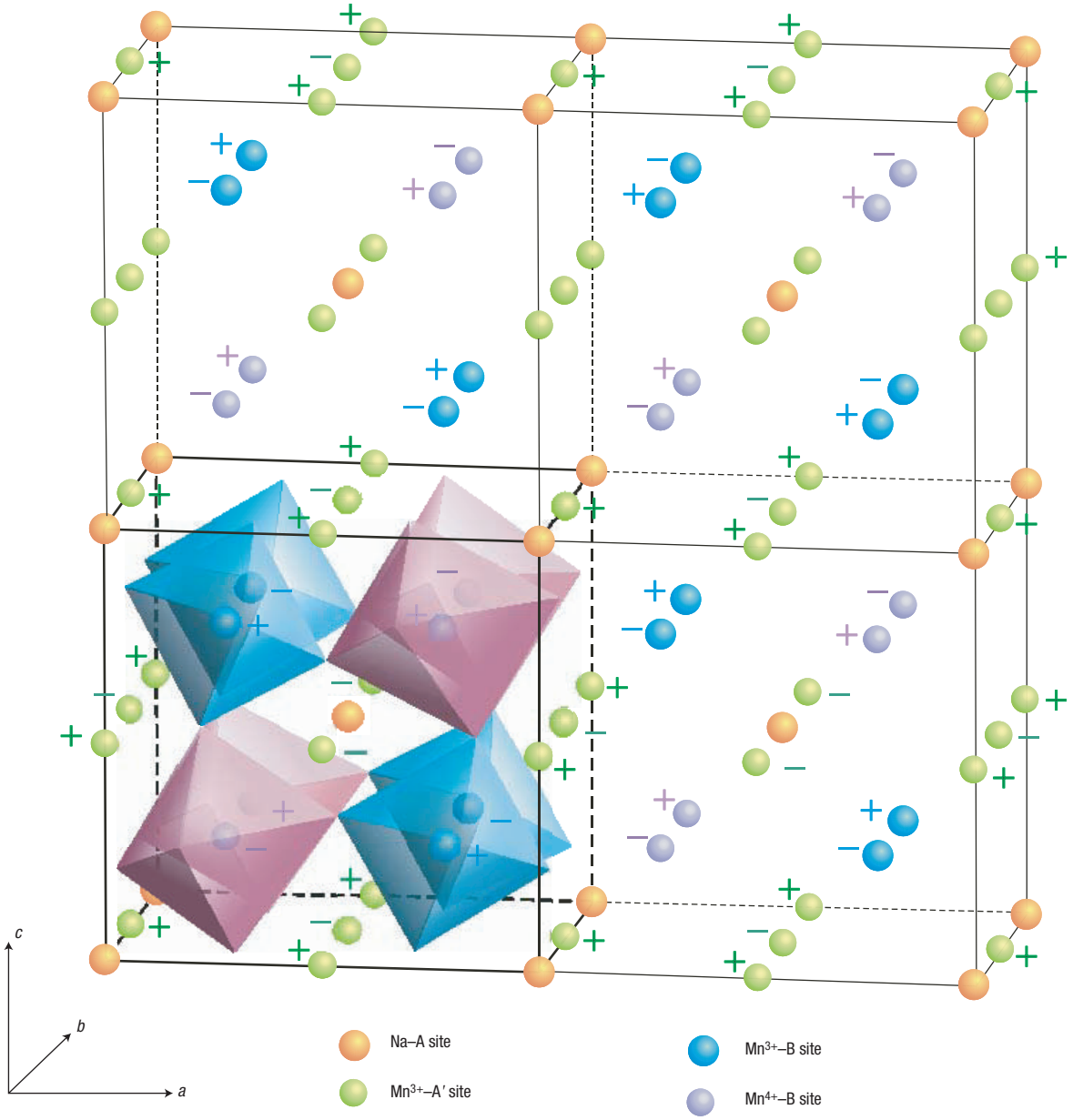

Figure 1 Crystal and magnetic structure of $(NaMn_3)Mn_4O_{12}$. The chemical unit cell of the double perovskite with *Im*3 symmetry is shown in the region containing the eight MnO_6 octahedra. The symmetry changes to *I*2/*m* at low temperature as a consequence of charge ordering, and the charge pattern is illustrated by different colours of the octahedra. The full cell, with doubling of the *a* and *c* axis, is needed to describe the CE-type magnetic structure of the Mn moments in the octahedral sites, whereas the anti-body centred magnetic structure of Mn^{3+} located on the A' sites has the same cell parameters as the nuclear one. The magnetic moments of Mn^{3+} on the A' sites lie in the *ac* plane, as do those of Mn^{3+} on the B sites. The moments of Mn^{4+} are parallel to the *c* axis. The ordering of the moments is represented by + and – signs.

coexists with the room-temperature phase down to the lowest temperatures measured (1.5 K)[5,6]. The structural analysis presented below suggests that this wide temperature range of two-phase coexistence[7] for the Ca-doped sample arises from the randomness introduced into the structure by doping.

The symmetry of the low-temperature phase of $(NaMn_3)Mn_4O_{12}$ is *I*2/*m* (in agreement with ref. 4), with the 12-coordinated Mn atoms split over the 2*b*, 2*c* and 2*d* positions, and the octahedrally coordinated Mn split over the 4*e* and 4*f* positions, and the Na located at the origin. Refinements of this structure at 150 K gave $a = 7.3527(6)$, $b = 7.1986(5)$, $c = 7.3493(6)$ Å, and $\beta = 90.558(3)°$, atomic positions for oxygen atoms: O(1): [–0.0104(7), 0.3097(8), 0.1804(8)], O(2): [0.1857(9), 0, 0.318(1)], O(3): [0.1754(9), 0, –0.3128(9)], and O(4): [0.3160(6), 0.1846(7), –0.0068(7)], with temperature factors 0.7(1), 0.1(1), and 0.45(3) $Å^2$ for A and B sites and O atoms, respectively, and excellent agreement between observed and calculated intensities ($R_p = 4.87\%$, $wR_p = 5.74\%$, and $\chi^2 = 1.081$). The average Mn(4*e*)–O and Mn(4*f*)–O distances of 1.986 and 1.910 Å and the corresponding bond valence sums of 3.28 and 3.92, respectively, show that the Mn^{3+} and Mn^{4+} ions are almost completely ordered in the length scale of the neutron diffraction

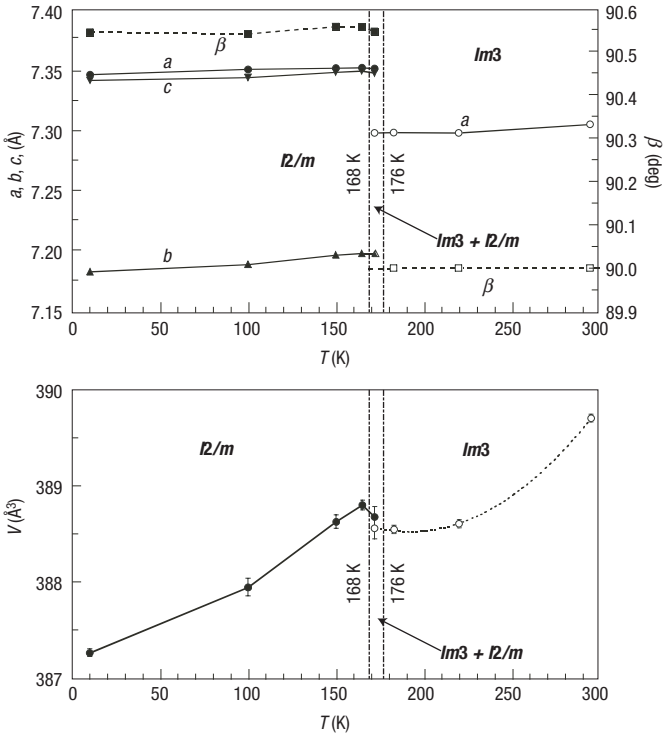

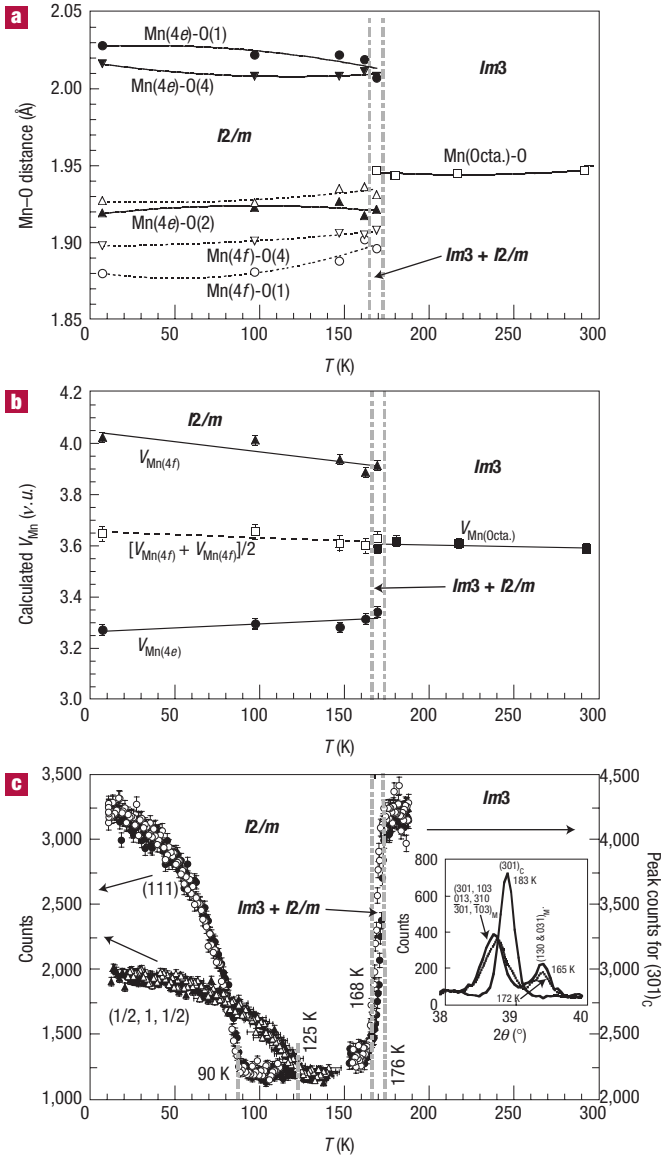

Figure 2 Temperature dependence of the cell parameters of $(NaMn_3)Mn_4O_{12}$. The discontinuities are discussed in the text. The powder neutron-diffraction experiments were performed by using the BT-1 high-resolution powder diffractometer located at the NIST Center for Neutron Research. Cu (311) and Ge(311) monochromators were used to produce monochromatic neutron beams of 1.5402, and 2.0775 Å wavelength, respectively. Collimators with horizontal divergence of 15′, 20′, and 7′ full-width at half-maximum were used before and after the monochromator, and after the samples, respectively. Open and solid symbols refer to the cubic, *Im*3 and monoclinic *I*2/*m* phases respectively. The right axis of the upper panel only relates to the squares, and indicates the cell angle β.

Figure 3 Structural and magnetic phase transitions. Neutron diffraction evidence of the three structural and magnetic phase transitions at (1) 176 K (cubic to monoclinic transition and Mn^{3+}/Mn^{4+} charge ordering); (2) 125 K (antiferromagnetic ordering of the Mn octahedral (B) sites); (3) 90 K (antiferromagnetic ordering of the Mn dodecahedral (A′) sites. **a**, Splitting of the 6 octahedral Mn–O distances at the charge-ordering transition 176 K. This splitting clearly differentiates the larger Mn^{3+} site from the smaller Mn^{4+} one in the Wyckoff positions 4*e* and 4*f* respectively. **b**, Corresponding changes of the volumes of the two MnO_6 octahedra. **c**, Temperature dependence of the intensity of the magnetic reflections (1,1,1) and (1/2,1,1/2). The data shown in this figure were obtained with the BT-7 triple-axis spectrometer (home-made at NIST) equipped with a pyrolytic monochromator and filter, and a neutron wavelength of 2.47 Å. The open and full symbols represent measurements on cooling and warming of the sample, respectively. The inset shows the splitting of the 301 cubic reflection.

experiment (~1,000 Å). The Mn–O distances for octahedrally coordinated Mn^{3+} (Mn^{4+}) ions in the 4*e* (4*f*) Wyckoff position are: 1.927(2), 2.009(5), and 2.023(5) Å (1.888(5), 1.935(2), and 1.906(5) Å). This points at a sizeable Jahn–Teller (JT) distortion on both sites that corresponds to an apical compression (elongation) of the $Mn^{3+}O_6$ ($Mn^{4+}O_6$) octahedra. At 150 K, the degree of the distortion is $\sigma_{JT} = 4.2 \times 10^{-2}$ Å, where $\sigma_{JT} \equiv (1/3\,\Sigma_i\,[(Mn–O)_i – \langle Mn–O \rangle]^2)^{1/2}$ (ref. 8). We conclude that, in $(NaMn_3)Mn_4O_{12}$, the occupied 3*d* orbitals of the Mn^{3+} ions are those with $x^2–y^2$ symmetry. This contrasts with half-doped manganites, where the orbital ordering is determined by incoherent Jahn–Teller distortions and incommensurate superstructures, and involves $3z^2–r^2$ orbitals[5,6,9]. The difference between the orbital ordering of $(NaMn_3)Mn_4O_{12}$ and that of half-doped manganites concerns not only the symmetry of the orbitals themselves, but also the pattern of this ordering in the *ac*-plane. This additional difference is due to the different *I*2/*m* symmetry.

In the 168–125 K range, only the paramagnetic *I*2/*m* phase is present (Fig. 3). Below 125 K, antiferromagnetic peaks develop, and can be accounted for by a model with a CE-type ordering of the magnetic moments associated with the octahedrally coordinated Mn cations, according to the classification originally proposed in ref. 10. As the temperature decreases, the magnetic intensities increase and then they tend to level off, as shown in Fig. 3. At about 92 K, new peaks appear that can be indexed in terms of the same unit cell of the nuclear structure in which the body centring has been eliminated. These new reflections are explained by a model in which the magnetic moments of the

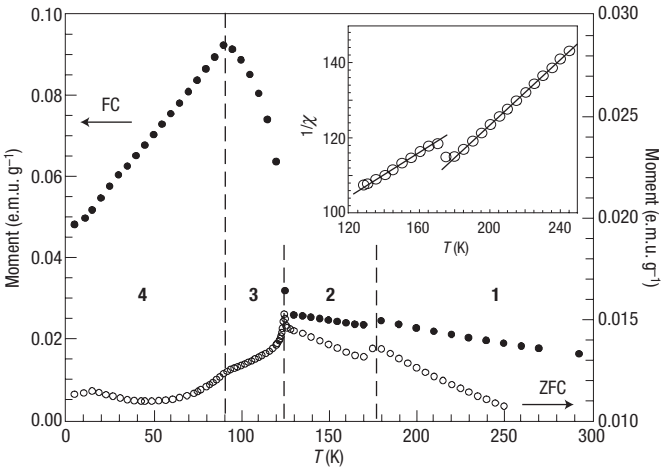

Figure 4 Temperature dependence of the d.c. magnetization. Zero-field cooling (ZFC) and field cooling (FC) curves in an external field of 100 Oe are shown (note the different scales). The various anomalies for these data are discussed in the text. The Curie-Weiss behaviour of the two paramagnetic regions 1 and 2 in the 125–300 K range is displayed in the inset. The solid lines are a guide for the eye.

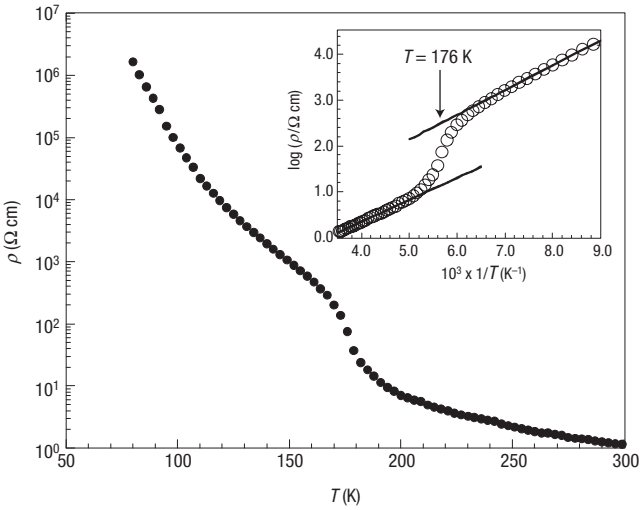

Figure 5 Temperature dependence of the resistivity. The d.c. resistivity shows the weakly insulating behaviour of $(NaMn_3)Mn_4O_{12}$. The thermally activated nature of the charge transport is evident from the Arrhenius plot in the inset, where solid curves are a guide for the eye. The linear fit yields an activation energy $E_a = 47$ meV, which remains nearly unchanged across the charge-ordering transition at 176 K.

12-coordinated Mn cations order antiferromagnetically with an anti-body-centred arrangement of the spins. The behaviour with temperature of the magnetic intensities of the CE and the anti-body-centred structures is shown in Fig. 3 for (1/2, 1, 1/2) and (1,1,1) respectively. The CE-type magnetic ordering observed in our compound is the same as that found in $La_{1/2}Ca_{1/2}MnO_3$ at low temperature. To better determine the magnetic structure, the structural refinement at 10 K was carried out using data taken at two neutron wavelengths, 1.5402 and 2.0785 Å (see Supplementary Information). The refined magnetic moments of $Mn^{3+}(4e)$ and Mn $^{4+}(4f)$ were found to be 2.85(4) and 2.40(4) μ_B (where μ_B is the Bohr magneton), respectively, that is, significantly lower than the values expected for a fully ordered arrangement, and comparable to those found at 1.5 K in $La_{1/2}Ca_{1/2}MnO_3$ (3.0 and 2.6 μ_B)[6]. This result indicates that the structural fluctuations present in the Ca-doped material do not significantly affect the behaviour of the magnetic moment in the CE structure, and the reduced moment may be due to spin transfer onto the oxygen. In the Ca-doped compound, the width of the magnetic peaks associated with the Mn^{3+} sublattice were greater than that of the peaks due to Mn^{4+}, which was attributed[5] to the size of the two sublattices caused by a twin operation that leaves the Mn^{4+} domains unchanged, while the size of the Mn^{3+} domains is reduced. No such feature is observed in the CE structure of $(NaMn_3)Mn_4O_{12}$, where the widths are all resolution limited. We conclude that the broad peaks observed in the Ca-doped system can be interpreted as a manifestation of the randomness caused by doping.

Magnetic and transport measurements were carried out in a radio frequency SQUID (superconducting quantum interference device) magnetometer equipped with a 5.5-T superconducting NbTi magnet. The magnetization curves, $M(T)$, were taken in both field- and zero-field-cooling (FC, ZFC) modes as a function of temperature. In Fig. 4 we show the ZFC and FC curves taken in a field of 100 Oe. As temperature is decreased, four distinct regions are observed. In the 300–125 K interval there exists two paramagnetic-like regions (1 and 2). The charge ordering at 176 K that differentiates the two regions reflects itself as a decrease of the slope of the χ^{-1} curve and as an abrupt increase of the absolute χ^{-1} value. A linear fit of this curve in the two regions yields Weiss constants of $\Theta_C = -54$ K and -190 K respectively. From 125 to 90 K (region 3), the ZFC curve exhibits an antiferromagnetic-like behaviour that turns into ferromagnetic-like in the FC curve. From 90 K down to 5 K (region 4), both ZFC and FC curves are antiferromagnetic-like. To make a quantitative analysis of the magnetic properties, we estimated the effective magnetic moment μ per unit cell from the Curie-law dependence in the two paramagnetic-like regions 1 and 2. In region 1, we obtained $\mu = 4.6 \pm 0.1\ \mu_B$ per Mn atom, consistent with the value of 4.7 μ_B per Mn atom expected from the ideal charge distribution of the formula $(NaMn^{3+}{}_3)(Mn^{3+}{}_2Mn^{4+}{}_2)O_{12}$. The wide temperature range, from 300 K to 176 K, of region 1 and the high degree of linearity of the χ^{-1} curve in this region makes the estimation very reliable. The more limited temperature 125–176 K range of region 2 does not allow us to draw definite conclusions. As no significant deviations from linearity in the χ^{-1} curve are observed, we should assume the validity of a simple Curie–Weiss picture also for this region. Under this assumption, the jump of χ^{-1} at 176 K indicates that the charge ordering is accompanied by an enhancement of the antiferromagnetic interaction between Mn ions. Indeed, the Weiss constant drops from −54 to −190 K. In addition, the decrease of the slope points at a sizeable increase of the effective magnetic moment up to $\mu \approx 6.1 \pm 0.1\ \mu_B$ per Mn atom. It follows that the picture of independent Mn ions is no longer valid for the charge-ordered paramagnetic phase. The moment increase can be explained by the appearance of Hund-type correlations among Mn ions leading to the formation of Mn pairs (or clusters). The underlying microscopic mechanism is not completely understood. A full answer to this point goes beyond the scope of this work, and awaits further experimental and theoretical efforts. We limit ourselves to recalling that a similar moment increase at the charge-ordering transition was reported in half-doped manganites[11], and explained in terms of Zener-type polarons[11,12] produced by the trapping of the $3d_{3z^2-r^2}$ electron within a pair of adjacent Mn ions. Such dynamic electron localization leads to an equal average valence of 3.5+ for both ions. This picture is incompatible with the charge order observed in our case, and an alternative model should be found. Another open question regarding the magnetic properties is raised by the ferromagnetic-like response of the system in the 90–125 K range as

the effect of cooling in low fields. Whether or not this peculiar response is linked to the discontinuity of χ^{-1} at 176 K remains to be established.

The resistivity, $\rho(T)$, was measured using a conventional d.c. technique in the four-probe (van der Pauw) configuration in the 300–80 K range (Fig. 5). At lower temperatures, the high sample resistance prevented reliable measurements. We note that $(NaMn_3)Mn_4O_{12}$ behaves as a weak insulator with room temperature resistivity $\rho(300\,K) = 1.2\,\Omega$ cm. At the temperature (176 K) corresponding to the structural phase transition, the resistivity suddenly increases, as observed in many mixed-valence compounds undergoing charge ordering, the classic example being magnetite[13]. Charge transport is thermally activated in the whole 300–80 K range studied, as indicated by the linear dependence of the Arrhenius plot in the inset of Fig. 5. Moreover, the activation energy E_a remains nearly unchanged on crossing the charge-ordering transition, and is found to be $E_a = 47$ meV, that is, of the order of the thermal energy at room temperature. No discontinuities correlated to magnetic orderings or sizeable magnetoresistive effects were observed in fields up to 5 T, contrary to the case of $CaCu_3Mn_4O_{12}$ (ref. 14). We conclude that the mechanism of charge transport is neither qualitatively nor quantitatively affected by the structural or magnetic phase transitions.

In conclusion, we have shown by direct crystallographic observations that $(NaMn_3)Mn_4O_{12}$, a double manganese perovskite-like oxide, exhibits mixed-valence behaviour at elevated temperatures and becomes fully charged and orbital ordered in the ground state. This contrasts with the behaviour of the doped compounds, where the structural inhomogeneities inherent in chemically substituted systems and the coexistence between the ordered and disordered phases do not permit the direct determination of the intrinsic charge and orbital ordering. The pristine nature of $NaMn_3Mn_4O_{12}$ makes it a model system for theoretical and further experimental studies.

Received 16 December 2002; accepted 17 November 2003; published 14 December 2003.

References

1. Marezio, M., Dernier, P. D., Chenavas, J. & Joubert, J.C. High pressure synthesis and crystal structure of $NaMn_7O_{12}$. *J. Solid State Chem.* **6,** 16–20 (1973).
2. Deschanvres, A., Raveau, B. & Tollemer, F. Remplacement de métal bivalent par le cuivre dans le titanates de type perowskite. *Bull. Soc. Chem. Fr.* **1967,** 4077–4078 (1967).
3. Collomb, A. *et al.* Neutron diffraction and magnetic properties of a series of ferrimagnetic oxides with the perovskite-like structure. *J. Magn. Magn. Mater.* **7,** 1–8 (1978).
4. Chenavas, J., Sayetat, F., Collomb, A., Joubert J. C. & Marezio, M. X-ray study of the low-temperature phase of $[NaMn^{3+}{}_3](Mn^{3+}{}_2Mn^{4+}{}_2)O_{12}$, a perovskite-like compound. *Solid State Commun.* **16,** 1129–1132 (1975).
5. Radaelli, P. G., Cox, D. E., Marezio, M.& Cheong, S.-W. Charge, orbital, and magnetic ordering in $La_{0.5}Ca_{0.5}MnO_3$. *Phys. Rev. B* **55,** 3015–3023 (1997).
6. Huang, Q. *et al.* Temperature and field dependence of the phase separation, structure, and magnetic ordering in $La_{1-x}Ca_xMnO_3$ (x=0.47, 0.50, and 0.53). *Phys. Rev. B* **61,** 8895–8905 (2000).
7. Moreo, A., Yunoki, S. & Dagotto, E. Phase separation scenario for manganese oxides and related materials. *Science* **283,** 2034 (1999).
8. Radaelli, P. G. *et al.* Structural effects on the magnetic and transport properties of perovskite $A_{1-x}A'_xMnO_3$ (x=0.25, 0.30). *Phys. Rev. B* **56,** 8265–8276 (1997).
9. Tokura, Y. & Nagaosa, N. Orbital physics in transition-metal oxides *Science* **288,** 462–468 (2000).
10. Wollan, E. O. & Koehler, W. C. Neutron diffraction study of the magnetic properties of the series of perovskite-type compounds $[(1-x)La, xCa]MnO_3$. *Phys. Rev.* **100,** 545–563 (1955).
11. Daoud-Aladine, A. *et al.* Zener polaron ordering in half doped manganites. *Phys. Rev. Lett.* **89,** 097205/1–4 (2002).
12. Zhou, J. S. & Goodenough, J. B. Zener versus De Gennes ferromagnetism in $La_{1-x}Sr_xMnO_3$. *Phys. Rev. B* **62,** 3834–3838 (2000).
13. Verway, E. J. W. Electronic conduction of magnetite (Fe_3O_4) and its transition point at low temperatures. *Nature* **144,** 327–328 (1939).
14. Zeng, Z., Greenblatt, M., Sunstrom IV, J. E., Croft, M. & Khalid, S. Giant magnetoresistance in $CaCu_3Mn_4O_{12}$–based oxides with perovskite-type structure. *J. Solid State Chem.* **147,** 185–198 (1999).

Acknowledgements

The authors thank T. Besagni and P. Ferro for technical assistance and acknowledge the CNR (Consiglio Nazionale delle Ricerche) for partial financial support within the framework of the National Project on 'Applicazioni della superconduttività ad alta T_c'.
Correspondence and requests for materials should be addressed to A.P.
Supplementary Information accompanies the paper on www.nature.com/naturematerials

Competing financial interests

The authors declare that they have no competing financial interests.